

Supporting Information

Scalable Synthesis of Colloidal CsPbBr₃ Perovskite Nanocrystals with High Reaction Yields Through Solvent and Ligand Engineering

Chun Kiu Ng,^{a,b} Wenping Yin,^{a,b} Hanchen Li,^{a,b} Jacek J. Jasieniak^{a,b,*}

^aARC Centre of Excellence in Exciton Science, Monash University, Clayton, VIC 3800, Australia.

^bDepartment of Materials Science and Engineering, Faculty of Engineering, Monash University, Clayton, VIC 3800, Australia.

Contents

1. TOL-LARP Synthesis of CsPbBr₃ Perovskite Nanocrystals

Figure S1. Antisolvents for precipitating PNCs in TOL-LARP crude solutions

Figure S2. Ligand solubility

2. EA-LARP Syntheses of CsPbBr₃ Perovskite Nanocrystals

Figure S3. EA-LARP optimization of the precursor:anti-solvent ratio

Figure S4. EA-LARP optimization of the ligand concentration

Figure S5. EA-LARP optimization of the OA:OLA ratio

Figure S6. EA-LARP optimization of the OA:OLA concentration

Figure S7. EA-LARP optimization of the purification

Figure S8. TOL/EA-LARP Tauc plots

Table S1. Absorption and PL properties

3. PLQY Measurements

4. AFM Measurements

Figure S9. AFM measurements

5. XRD Measurements

Table S2. SAED reflections

Figure S10. XRD for TOL/EA-LARP

6. DLS Measurements

Figure S11. DLS measurements

7. ICP-MS Preparation

8. CsPbBr₃ Molar Extinction Coefficient Calculation

Table S3. CsPbBr₃ Molar Extinction Coefficient

9. Time Dependent Measurements

Figure S12. TD-Abs measurements for Tauc plots

Figure S13. TD-Abs measurements with multiple injections

Figure S14. PL measurements with multiple injections

Figure S15. Spontaneous precipitation in EA-LARP crude solution

10. ¹H NMR Spectroscopy

Figure S16. NMR Spectroscopy of TOL/EA-LARP PNCs

11. FTIR Spectroscopy

Figure S17. FTIR spectra of TOL/EA-LARP PNCs using OLA

12. Post-Synthetic Treatments to CsPbBr₃ PNCs

Figure S18. Normalized PL spectra of C₁₂NH₃Br additions to TOL/EA-LARP

13. EA-LARP Syntheses with Primary Saturated Alkylamines

Figure S19. Photographs of crude/purified EA-LARP solutions with saturated primary amines

Figure S20. Saturated primary ammonium-oleate solubility

Figure S21. Abs/PL of EA-LARP with saturated primary amines

Table S4. Estimation of perovskite content of EA-LARP with saturated primary amines

Table S5. Absorption and PL properties of EA-LARP with saturated primary amines

Figure S22. Stability of LARP PNCs over a week without ligand additions

Figure S23. Stability of LARP PNCs over a week with different C_8NH_3Br additions

Figure S24. XRD films of EA-LARP w/ primary amines

14. Upscaling EA-LARP

Figure S25. Photographs of upscaled synthesis

15. Halide Exchange

16. References

1. TOL-LARP Synthesis of $CsPbBr_3$ Perovskite Nanocrystals

For TOL-LARP, a metal halide precursor stock solution (typically 10 mL) was prepared within a glovebox containing 0.040 M of CsBr and 0.040 M of $PbBr_2$ in anhydrous DMF. This solution was stirred under 80 °C heating to ensure full solubilization and stored in ambient conditions. When required, this DMF metal halide solution was added to glass vials containing 10 v/v % (0.317 M) of OA and 5 v/v % (0.152 M) OLA from their degassed stock solutions. The DMF solution, now containing both metal halides and ligands, was gently heated to 80 °C to ensure a homogeneous and transparent solution. Otherwise, the solution is partially opaque at room temperature and the more viscous ligands stick to the sides of glass vials. The warm solution was then injected dropwise at $\sim 75 \mu\text{L/s}$ into the vigorously stirred toluene anti-solvent at a DMF:TOL ratio of 1:10 for 2 min. Afterwards, the crude PNC solution was transferred to 50 mL centrifuge tubes, with EA added in a 1:3 ratio to enhance precipitation, to be centrifuged at 8000 rpm for 5 min. The supernatant was then decanted and the pellet re-dispersed with a volume of toluene that was equivalent to the DMF precursor volume used in the crude solution. This was then centrifuged a second time at 3000 rpm for 2 min. The supernatant was used for purified $CsPbBr_3$ characterizations and stored under dark ambient conditions with the remaining pellet discarded.

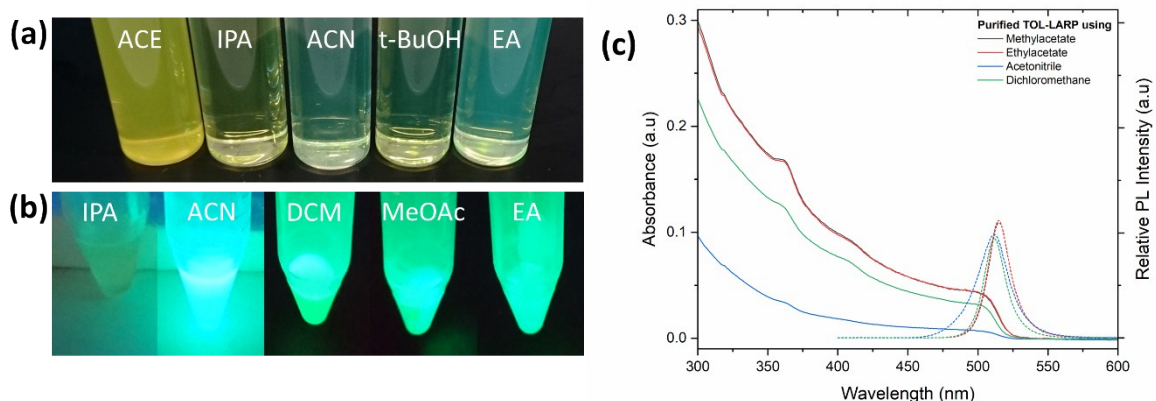


Figure S1. (a) Lab images under ambient light of acetone, isopropanol, acetonitrile, tert-butanol and ethyl acetate mixed with TOL-LARP crude $CsPbBr_3$ PNC solutions to enhance precipitation. Acetone notably resulted in immediate aggregation and quenching of its PL, rendering it unsuitable. (b) The toluene re-dispersed PNCs post-centrifugation for more suitable solvents of isopropanol, acetonitrile, dichloromethane, methyl acetate and ethyl acetate. Isopropanol also resulted in aggregation as with acetone, while acetonitrile contained very low yields of PNCs (note, these two samples are photographed being much closer to $\lambda = 365 \text{ nm}$ UV light source). Dichloromethane, methyl acetate and ethyl acetate retain fluorescent PNCs. (c) Absorbance spectra of the final purified solutions at the same dilution factor, showing the relative PNC yields with different solvents for purification.

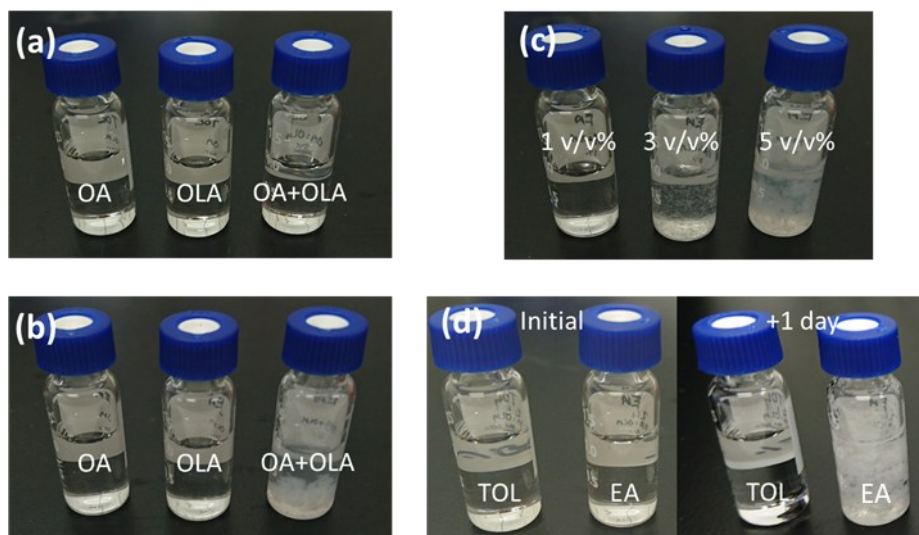


Figure S2. Solubility tests of OA, OLA and OA+OLA in (a) TOL and (b) EA, with additions of 20 v/v% OLA (left), 20 v/v% OA (middle), 20v/v% OA+OLA (right); the oleylammonium-oleate salt in EA is the only sample which results in precipitates. (c) Additions of OA+OLA in EA at 1 v/v% (left), 3 v/v% (middle), 5 v/v% (right), with precipitates becoming more visible at higher concentrations. (d) Ligands added separately to form 20 v/v% OA+OLA in TOL (left) and EA (right) with precipitation from the resultant ligand salt occurring in EA within hours.

2. EA-LARP Syntheses of CsPbBr₃ Perovskite Nanocrystals

Initial tests directly substituting EA for TOL in the optimized TOL-LARP protocol, a morphological trend with the DMF:EA ratio was found. At a low ratio of 1:10, a mixture of nanocuboids (NCu) and nanoplatelets (NPL) 3-5 unit cells thick formed.¹ As the ratio increased up to 1:30, only NCu formed (Figure S3). Further investigation into the DMF:EA reaction ratio found that a ratio of 1:15 was the most conducive for good yields of homogeneous NCu crystals with relatively high PL emissions with narrow fwhm. (Figure S4). Decoupling the relative molar ratios of the metal halide salts and organic ligands was found to provide further control over the CsPbBr₃ PNCs. At high OLA quantities (>0.15 M), NPL are the dominant product. For decreasing OLA content, a transition to a mixed NPL-NCu morphology and then to a NCu morphology is observed at [OLA] < 0.06 M (Figure S5a,b). Meanwhile, an OA:OLA ratio of 2:1 is found to be sufficient to protonate OLA to the surface-binding OLA⁺ species, with higher OA ratios resulting in no synthetic benefit (Figure S5c-d). Systematic variations of the total concentration of 2:1 OA:OLA ligands at 0.5 v/v % intervals reveals that the optimal ligand concentration is 4 v/v % (0.127 M) and 2 v/v % (0.061 M) for OA and OLA, respectively. Above this ligand concentration, the CsPbBr₃ solutions tended to be more polydisperse and exhibit mixed NPL-NCu morphologies. Below this concentration, the majority of crystals were colloidal unstable due to their large size. Notably, this is 40 % of the ligand concentration relative to that used for TOL-LARP, which displayed similar absorption and PL spectra (Figure S6). The effects of the purification process on the PNCs has also been investigated and further optimized. A decreasing trend in PL intensity for higher centrifugation speeds is observed (Figure S7). This is consistent with previous reports where the desorption of ligands from the crystal surface were a noted consequence of centrifugation.² The final optimized EA-LARP protocol follows the TOL-LARP procedures as outlined in Section 1 with the described changes in the main Experimental Section.

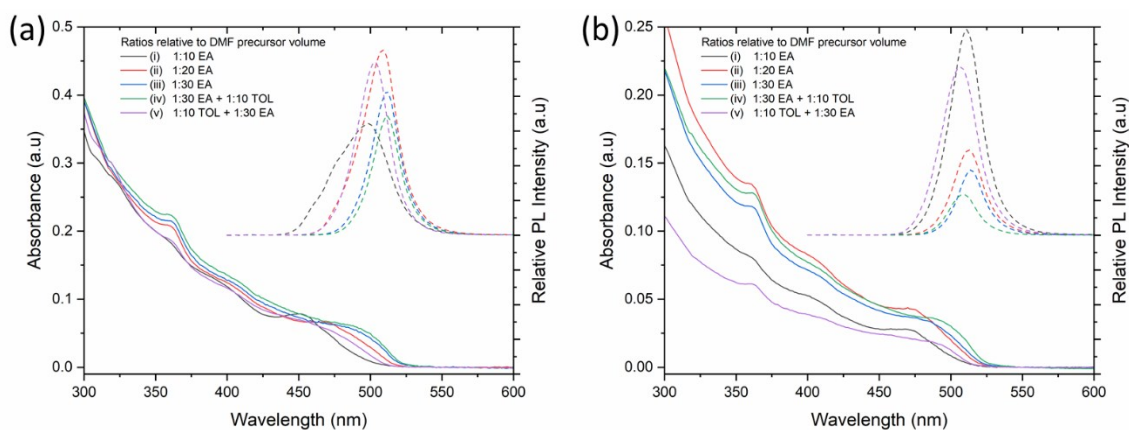


Figure S3. The recorded absorption and PL spectra of the EA-LARP (a) crude and (b) purified solutions; (i-iii) are directly centrifuged without further solvent additions once the reaction had been completed; (v) represents the standard TOL-LARP reaction with EA added after the reaction, and the reverse, (iv) where TOL is similarly added into the EA-LARP reaction mixture.

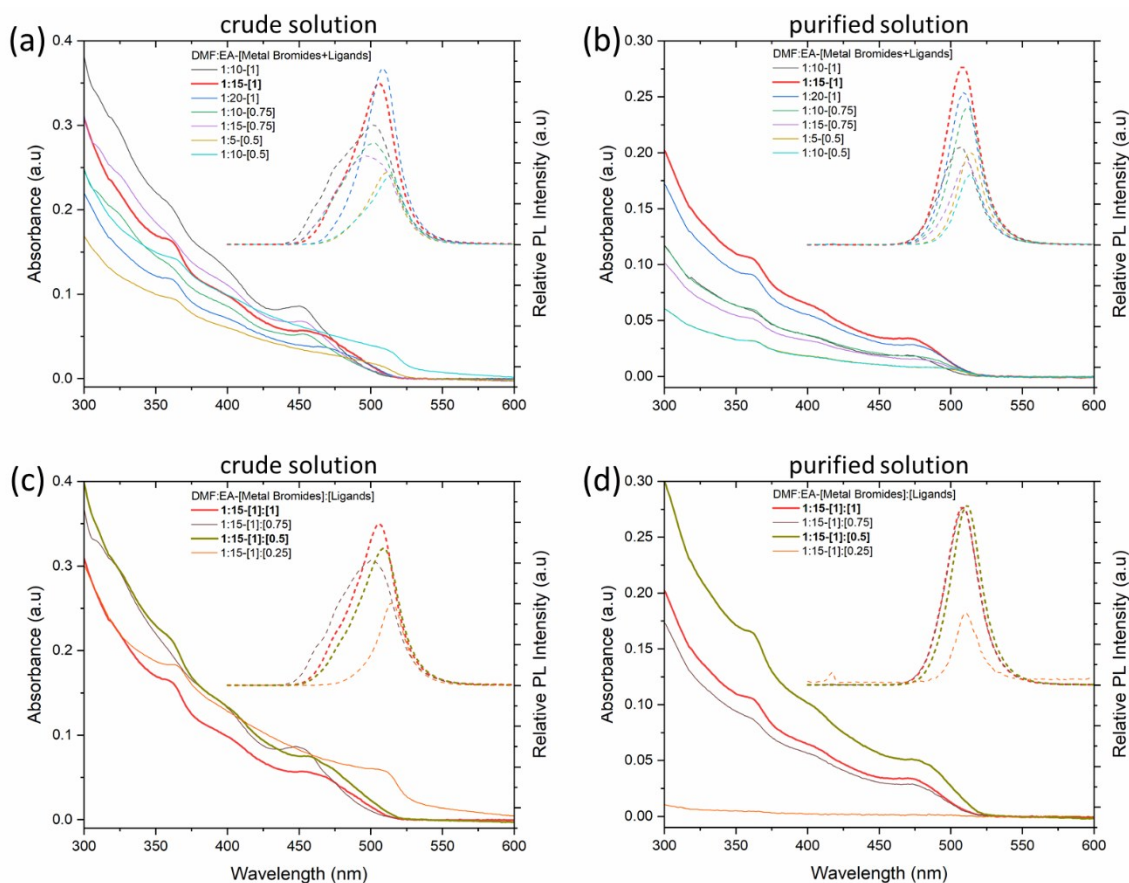


Figure S4. The recorded absorption and PL spectra of the (a) crude and (b) purified solutions with different DMF:EA reaction ratios and the diluted DMF precursor concentration relative to TOL-LARP. The recorded absorption and PL spectra of the (c) crude and (d) purified solutions with a DMF:EA reaction ratio of 1:15 with various ligand concentrations while the metal halide concentration remains constant. Promising combinations are in bold.

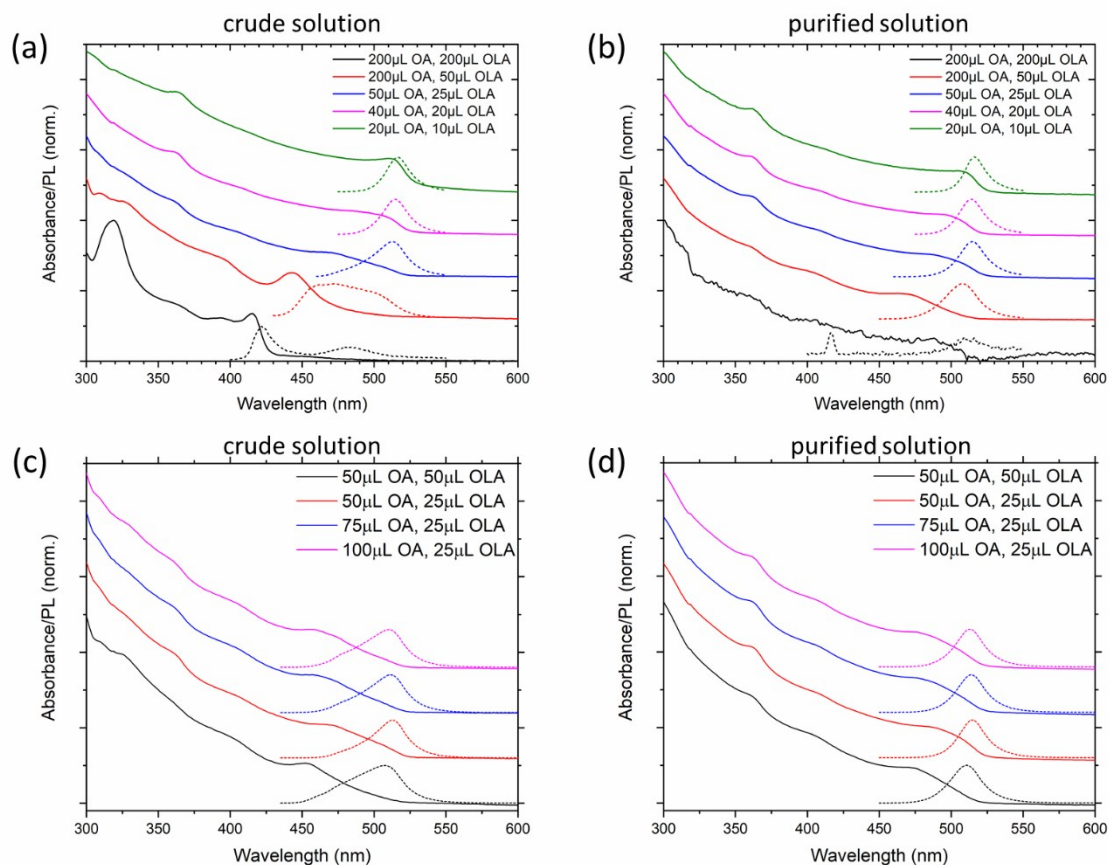


Figure S5. The normalized absorption and PL spectra of EA-LARP (a) crude solutions showing the range of different NPL/NCu morphologies that are possible through ligand control, and their (b) purified solutions which were optimized for obtaining NCu. The EA-LARP (c) crude and (d) purified solutions demonstrating the negligible effects of higher acid:amine ratios, and that the amount of OLA is a stronger influencing factor on morphology. The DMF:EA ratios are 1:15 and ligand volumes are relative to 1.0 mL of DMF precursor with 0.040 M CsBr and PbBr₂.

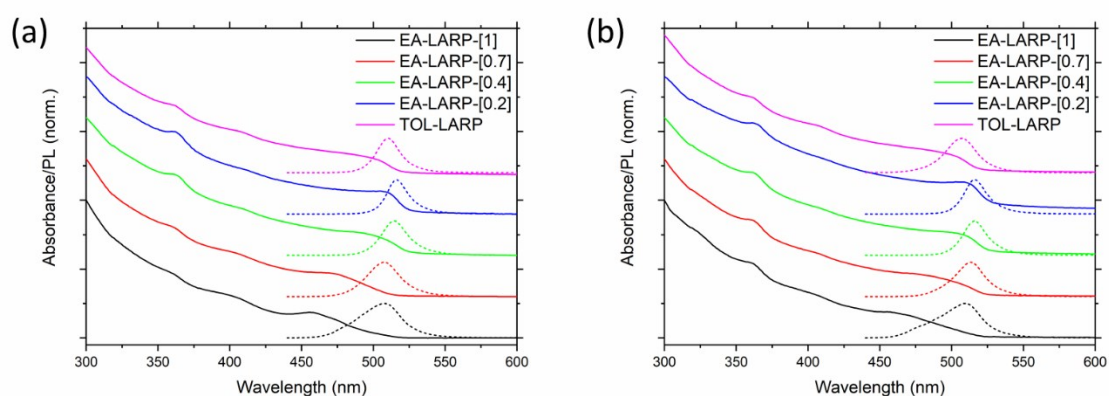


Figure S6. The normalized absorption and PL spectra of (a) crude and (b) purified LARP solutions, with a series of EA-LARP variants spanning the trialed ligand concentrations of OA:OLA in a 2:1 ratio.

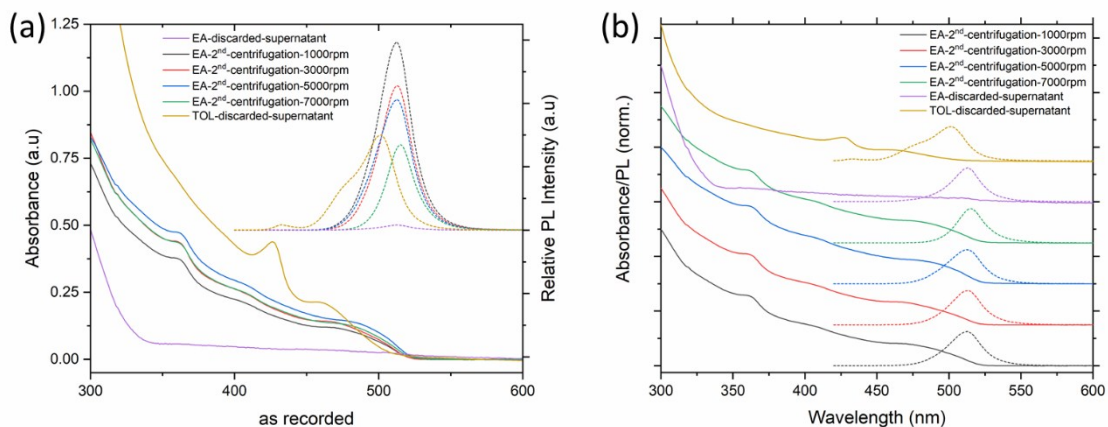


Figure S7. The (a) as-recorded and (b) normalized absorption and PL spectra of TOL/EA-LARP's discarded supernatant without any dilution and the purified PNC solutions of EA-LARP with different speeds for the second centrifugation step at the same dilution factor.

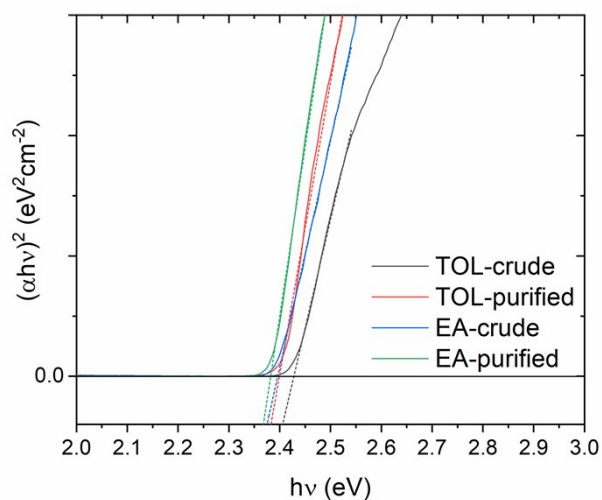


Figure S8. Tauc plots calculated from the TOL/EA-LARP absorbance from Figure 2a,b. The estimated bandgap values are presented in Table S1.

Table S1. Summarization of absorption and PL properties of TOL/EA-LARP solutions.

	TOL-crude	TOL-purified	EA-crude	EA-purified
PL Peak (nm)	507	511	514	516
PL fwhm (nm)	26	19	25	22
PLQY (%)	–	25	–	21
Abs onset (nm)	~520	~520	~525	~525
Abs 1 st excitonic peak (nm)	~490	~505	~480	~494
Bandgap Energy (eV)	~2.43	~2.40	~2.39	~2.38
CsPbBr ₃ Reaction Yield (%)	82.2	17.9	93.4	40.2
PNC mass per waste volume (mg/mL)	–	0.10	–	0.62

3. PLQY Measurements

The PLQY of PNCs were determined from the calibration curve of Rhodamine-6G dye in anhydrous ethanol (QY = 0.95) at an excitation wavelength of 470 nm.³ This was calculated with the equation:

$$Q_s = Q_r \left(\frac{A_r}{A_s} \right) \left(\frac{I_s}{I_r} \right) \left(\frac{n_s}{n_r} \right)^2 \quad (1)$$

Where: Q is the fluorescence quantum yield, A is the absorbance, I is the integrated fluorescence intensity, n is the refractive index of the solvent. Subscripts 'r' and 's' refer to the reference and sample, respectively.

4. AFM Measurements

1 inch² silicon substrates were sonicated in acetone, then isopropanol and plasma cleaned for 10 min at each step. The purified CsPbBr₃ PNC solutions were then spun casted at 2000 rpm for 60 s.

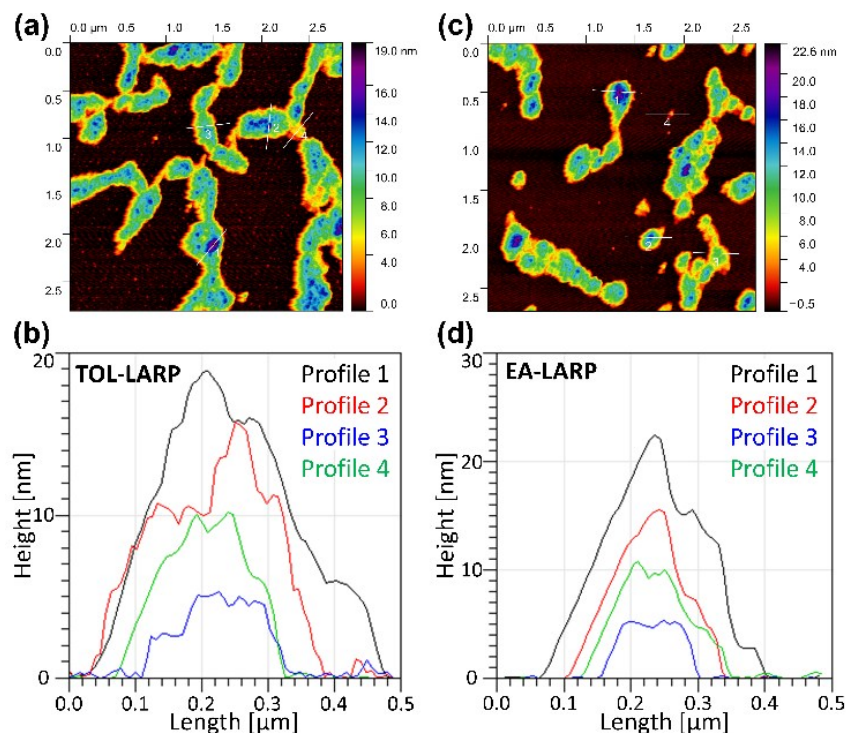


Figure S9. (a) AFM measurements of TOL-LARP PNCs deposited on silicon substrates with the (b) cross-section height profiles showing 1-4 layers of PNCs. (c,d) This is similarly shown for EA-LARP synthesized PNCs.

5. XRD Measurements

Several hundred microliters of the purified CsPbBr₃ PNC solution were deposited on a glass substrate (sonicated in acetone, then isopropanol for 10 min each). The toluene solvent was dried off at ~30 °C under gentle gas flow.

Table S2. SAED patterns with calculated d-spacings for major reflections (± 0.04 and ± 0.03 Å in d-spacing for TOL/EA-LARP, respectively).

Tol-LARP d(Å)	Cubic plane (hkl)	Cubic d(Å) ref.	Ortho plane (hkl)	Ortho d(Å) ref.
5.872	100	5.830	020	5.877
4.124	110	4.122	121/200	4.134
2.937	200	2.915	040/202	2.923
2.641	210	2.607	222/301	2.607
2.398	211	2.380	240/042	2.391
2.070	220	2.061	242	2.067
1.869	310	1.844	402	1.843
1.464	400	1.458	080/404	1.462
1.302	420	1.304	444	1.303
EA-LARP d(Å)	Cubic plane (hkl)	Cubic d(Å) ref.	Ortho plane (hkl)	Ortho d(Å) ref.
5.871	100	5.830	020	5.876
4.118	110	4.122	121/200	4.134
2.917	200	2.915	040/202	2.923
2.638	210	2.607	222/301	2.607
2.383	211	2.380	240/042	2.390
2.069	220	2.061	242	2.067
1.841	310	1.844	402	1.842
1.463	400	1.458	080/404	1.461
1.290	420	1.304	444	1.303

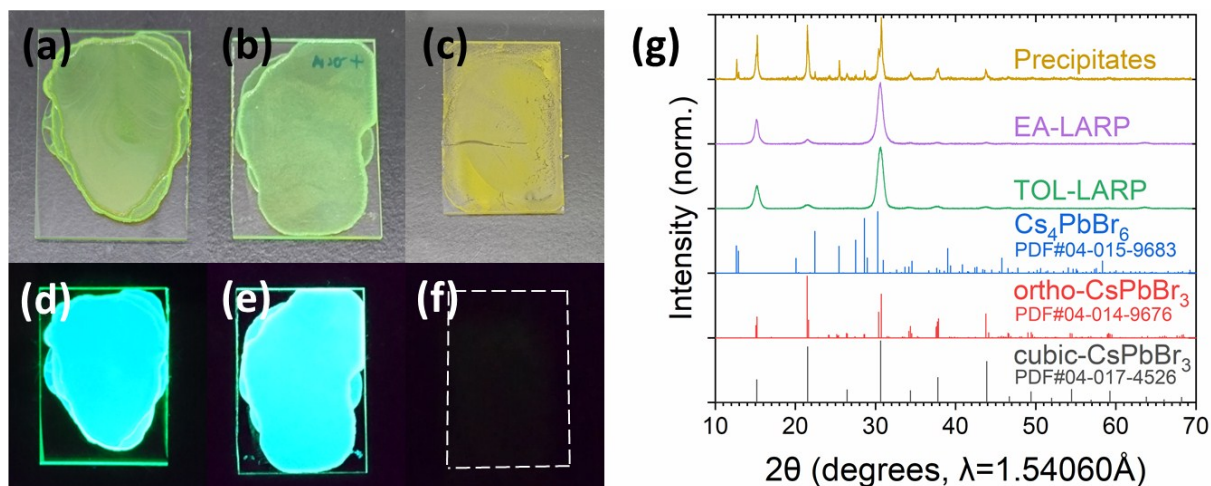


Figure S10. Photographs of XRD films of purified CsPbBr₃ from (a,d) TOL-LARP, (b,e) EA-LARP and (c,f) non-emissive precipitates under (top row) ambient light and (bottom row) $\lambda = 365$ nm UV-light. The purified samples' (a,b) XRD spectra for matches closely with PDF#00-054-0752, possessing the standard space group of $Pm-3m$ and unit cell dimensions of $a = b = c = 5.83$ Å. The non-colloidally stable, non-emissive precipitates of the reaction (c) were found to be highly orthorhombic (γ -CsPbBr₃) in nature, which matches with PDF#01-085-6500, possessing the standard space group of $Pnma$ with unit cell dimensions of $a = 8.250$ Å, $b = 11.753$ Å, $c = 8.203$ Å. Furthermore, minor amounts of rhombohedral 0D Cs₄PbBr₆ peaks were also detected through its characteristic double peak at $2\theta = 12.6^\circ$ and 12.9° , matching with PDF#04-015-9683, possessing a space group of $R-3c$ which exhibits unit cell dimensions of $a = b = 13.722$ Å, $c = 17.315$ Å. (g) The XRD patterns of the respective films and reference spectra.

6. DLS Measurements

To minimize ligand desorption and subsequent aggregation, the CsPbBr₃ PNCs were diluted into toluene with OLABr at 0.02 mg/mL. A series of solutions were tested with dilution factors of ~333-33 for the crude and purified samples of TOL-LARP, EA-LARP and HI was performed to find the dilution factor that had the least aggregation without changes to its optical properties. HI synthesized samples followed the procedure as described by Protesescu et al.⁴

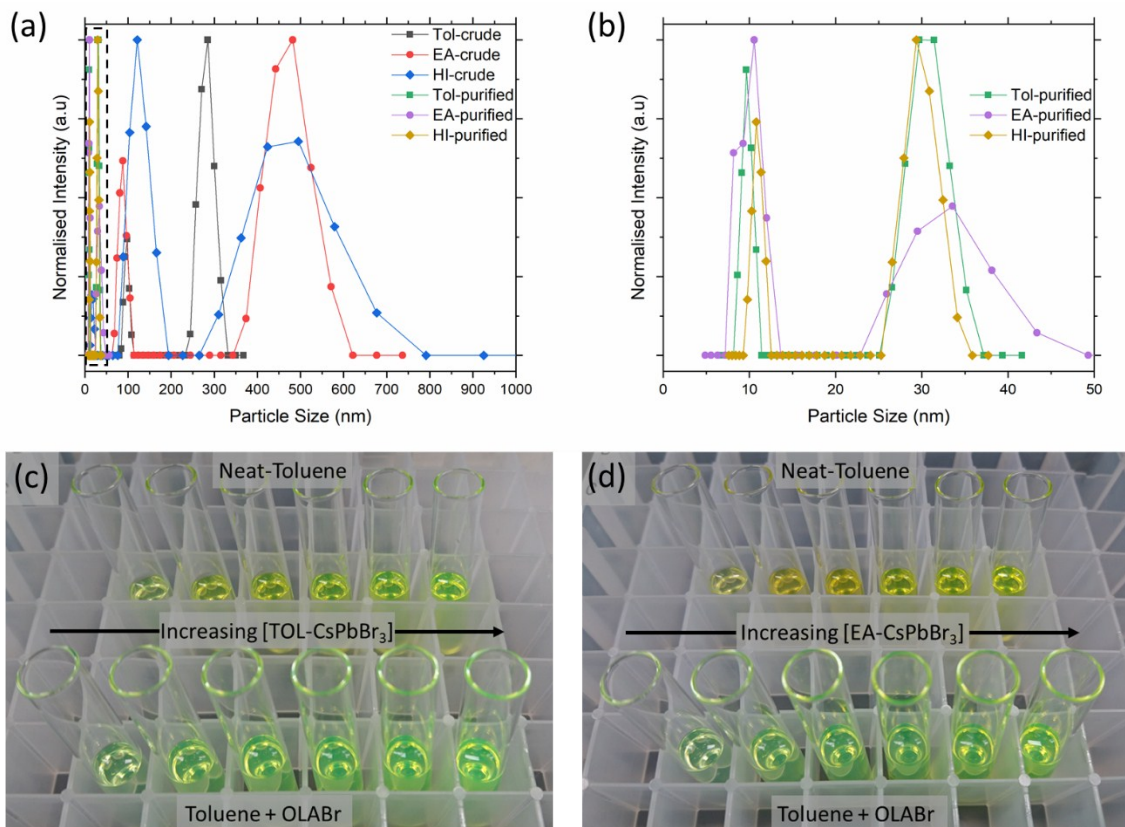


Figure S11. (a) Dynamic light scattering measurements of TOL/EA-LARP crude and purified solutions, with HI-synthesized CsPbBr₃ crude and purified solutions as a reference for comparison. (b) Enhancement of the smaller ~10 nm particle size peaks of Figure S11a. A series of purified CsPbBr₃ PNC solutions at increasing concentrations in (top row) neat-toluene and (bottom row) 0.02 mg/mL OLABr in toluene for (c) TOL-LARP and (d) EA-LARP. These show particle radius estimates of ~9.6 and ~10.6 nm for TOL-LARP and EA-LARP samples, respectively. The reference HI CsPbBr₃ PNCs measured similar particle sizes of ~10.8 nm. The ~15 % overestimation of particle size from DLS is not unexpected, as the nature of the measurement only provide an equivalent hydrodynamic radius that is representative of the dispersed PNCs. Nevertheless, the supporting particle size estimates with DLS confirm that EA-LARP PNCs are slightly larger than their TOL-LARP counterparts.

7. ICP-MS Preparation

Purified CsPbBr₃ PNCs in toluene were diluted with acetonitrile and a known amount of Rh and In internal standard. Each flask was placed in an ultrasonic bath for 5-10 minutes to break up any solids that formed. ICP-MS Calibration standards were prepared with matrix matched acetonitrile and Rh/ In internal standards.

8. CsPbBr₃ Molar Extinction Coefficient Calculation

The collected ICP-MS and absorbance measurements followed the same experimental derivation of the molar extinction coefficient (ϵ) as described by De Roo et al.⁵ The intrinsic absorption coefficient (μ_i) is given by equation (1):

$$\mu_i = \frac{\ln(10)A}{fL} \quad (1)$$

Which is dependent on the absorbance (A) at a particular wavelength, the optical pathlength where $L = 1$ and volume fraction which is given by equation (2):

$$f = \frac{c \times N_A \times a^3}{10^{24}} \quad (2)$$

Which is dependent on the concentration (c), Avagadro's number (N_A) and the CsPbBr₃ cubic lattice spacing $a = 0.587$ nm. These can then be incorporated into the final equation (3) below to calculate ϵ , where d represents the cube edge length in nanometers.

$$\epsilon = \frac{N_A \mu_i}{\ln(10)} d^3 \quad (3)$$

The key calculated values are shown in Table S3 below, and similar to previous reports.^{5,6} Using the differences in the [Cs] and [Pb] as the margin of error, the final $\epsilon_{(335\text{nm})}$ value for TOL- and EA-LARP is $(0.052 \pm 0.004)d^3$ and $(0.051 \pm 0.005)d^3 \text{ cm}^{-1}\mu\text{M}^{-1}$. The molar extinction coefficient can then be calculated for different crystal sizes and then be used to determine their concentration from their measured absorbances.

Table S3: Summary of the CsPbBr₃ molar concentration from ICP, the absorbance of the analyzed PNC solutions, the derived volume fraction of CsPbBr₃, the intrinsic absorption coefficient and molar extinction coefficient, where d represents the cube edge length in nm.

Sample	[Cs,Pb] (mmol/L)	f (a.u)	A _(335nm) (a.u)	$\mu_{i,(335\text{nm})}$ (cm ⁻¹)	$\epsilon_{(335\text{nm})}$ (cm ⁻¹ μM ⁻¹)
Tol-LARP	5.06E-05	6.17E-06	0.533	1.99E+05	0.0520 d^3
EA-LARP	5.75E-06	2.33E-06	0.197	1.95E+05	0.0509 d^3
Hot-Injection	9.16E-06	3.63E-06	0.304	1.93E+05	0.0506 d^3
Reference ⁵	–	–	–	1.98E+05	0.0518 d^3
Reference ⁶				1.79E+05	0.0474 d^3

9. Time Dependent Measurements

For the single injection TD-Abs/PL measurements, measurements were conducted within quartz cuvettes filled with 3.0 mL of TOL or EA which were constantly stirred at 2000 rpm with a small stirrer bar. To adapt the LARP reactions to this apparatus, 10 μL of the TOL-LARP DMF precursor was added to the two anti-solvents. A significantly lower reaction ratio of 1:300 was required to maintain compatibility with the detectors (i.e. avoid significant noise, scattering or saturating the detector). An unavoidable consequence of this, is that the ligand concentration of the formed crude PNC solution is drastically lower than usual. This significantly affected the EA-LARP reaction the most, which saw uncontrolled crystal growth. This is because its optimized precursor composition is at the threshold ligand concentration for ensuring controlled growth. To address this ligand deficiency, the TD measurement for EA-LARP uses the same DMF precursor composition as for TOL-LARP.

For the multiple injection TD-Abs measurements, conditions were as above for the single injection but five 10 μL precursor injections were made in 20 s intervals. The 450 nm region was selected to be tracked over time as it was a spectral region free of morphological dependent features of excessive noise. For the corresponding PL measurements, it was collected with the Horiba Fluoromax-4 Spectrofluorometer for its better resolution and sensitivity. This also allowed the use of EA-LARP's DMF precursor for measurements, instead of requiring TOL-LARP's precursor with higher ligand content.

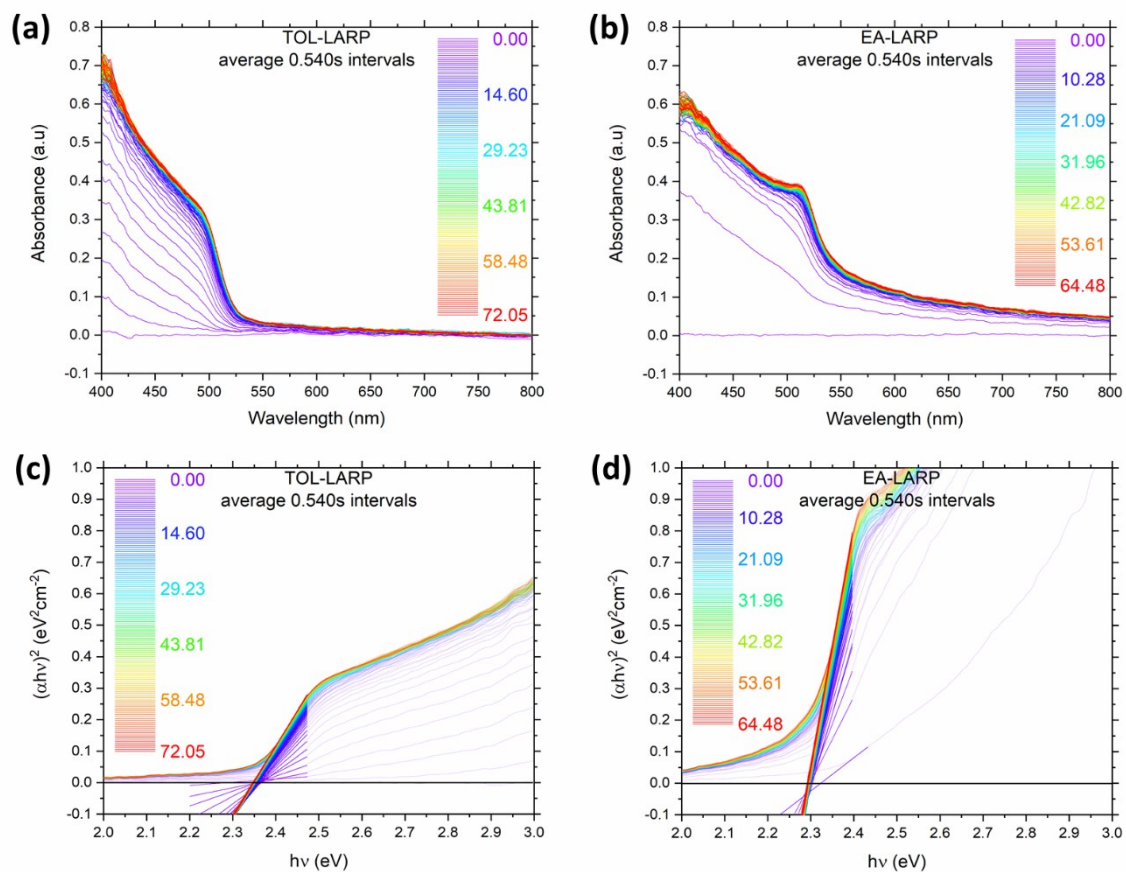


Figure S12. The TD-Abs spectra of (a) TOL-LARP and (b) EA-LARP CsPbBr₃ crude mixtures at 4 ms integration times to reduce signal-to-noise levels. (c,d) Tauc plots calculated from the TOL/EA-LARP absorbance from Figure S12a,b.

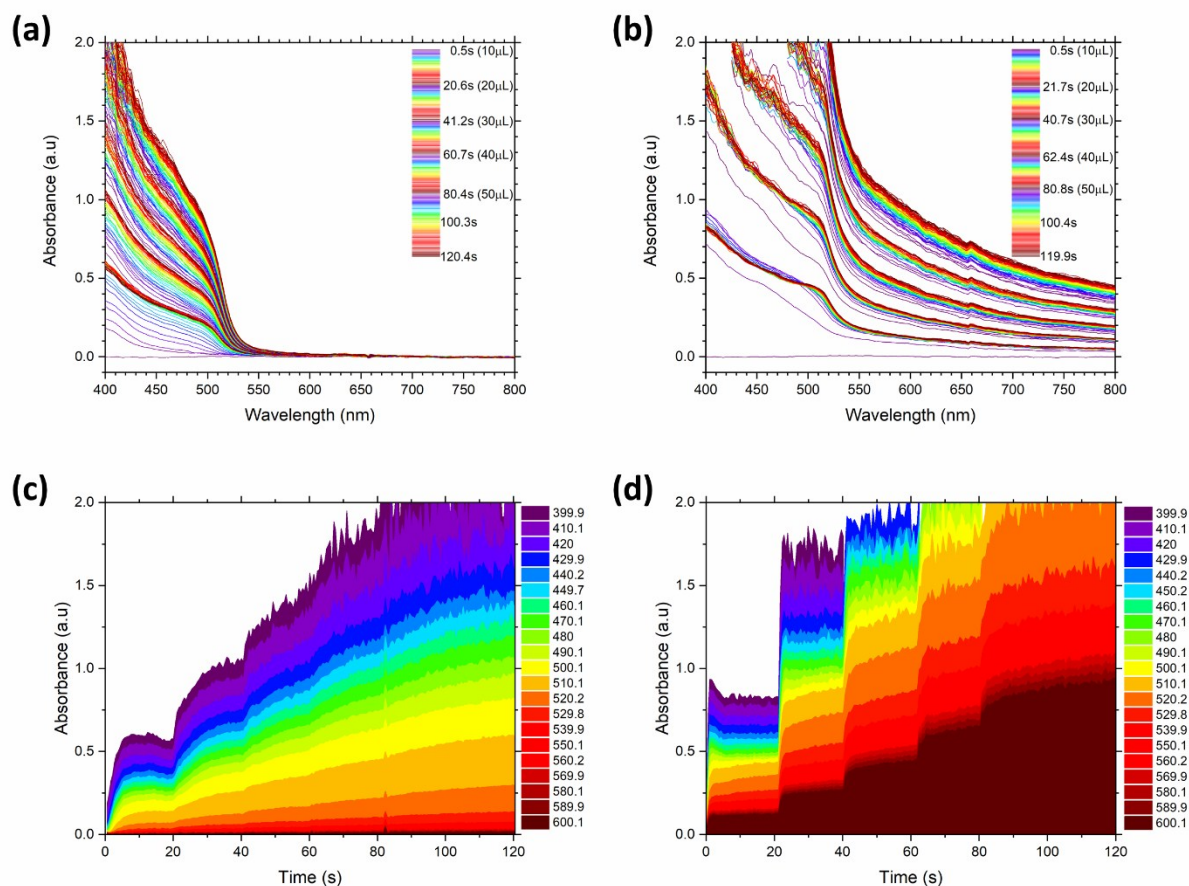


Figure S13. The TD-Abs spectra where 10 μL of TOL-LARP's DMF precursor is added in five 20 s intervals to a stirred 3.0 mL solution of (a) TOL and (b) EA. (c,d) The absorbance of different wavelengths plotted against time from Figure S13a,b respectively. EA-LARP reaction uses $\times 2.5$ its typical ligand content (i.e. same precursor composition as for TOL-LARP).

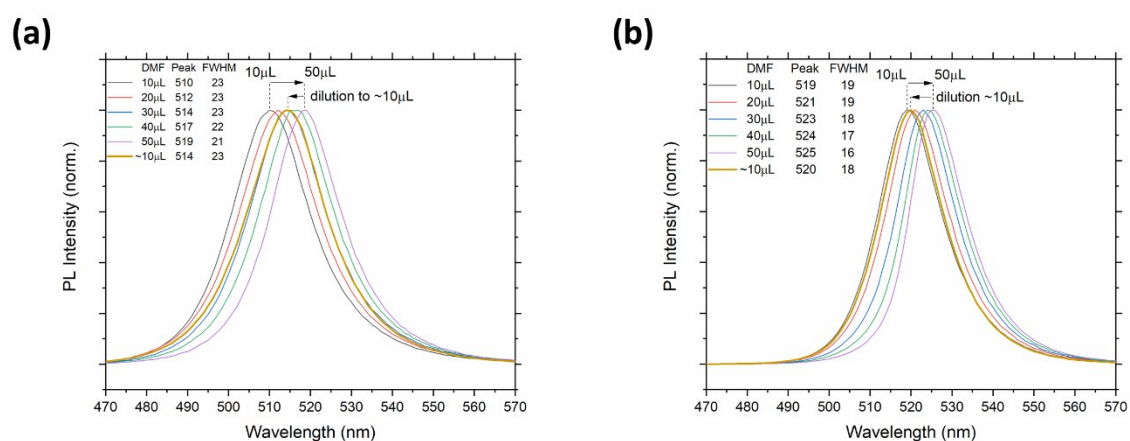


Figure S14. (a) The PL spectra of TOL-LARP, where its DMF precursor is added in five sequential 10 μL additions. After this, it is diluted five-fold, giving an equivalent DMF:TOL ratio to when 10 μL of DMF precursor was first added. (b) This is similarly shown for EA-LARP with its own precursor.

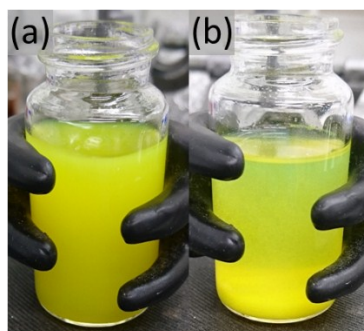


Figure S15. (a) Freshly synthesized EA-LARP crude solution. (b) Crude solution left standing for 60 s showing definitive particle separation under gravitational forces without the need of an additional solvent or centrifugation.

10. $^1\text{H-NMR}$ Spectroscopy

Proton nuclear magnetic resonance ($^1\text{H-NMR}$) spectroscopy was performed on purified CsPbBr_3 samples dispersed in toluene- d_8 . Purified samples were twice dried under high vacuum and re-dispersed with a small amount of toluene- d_8 before being finally dried and re-dispersed at the final concentration for $^1\text{H-NMR}$ analysis.

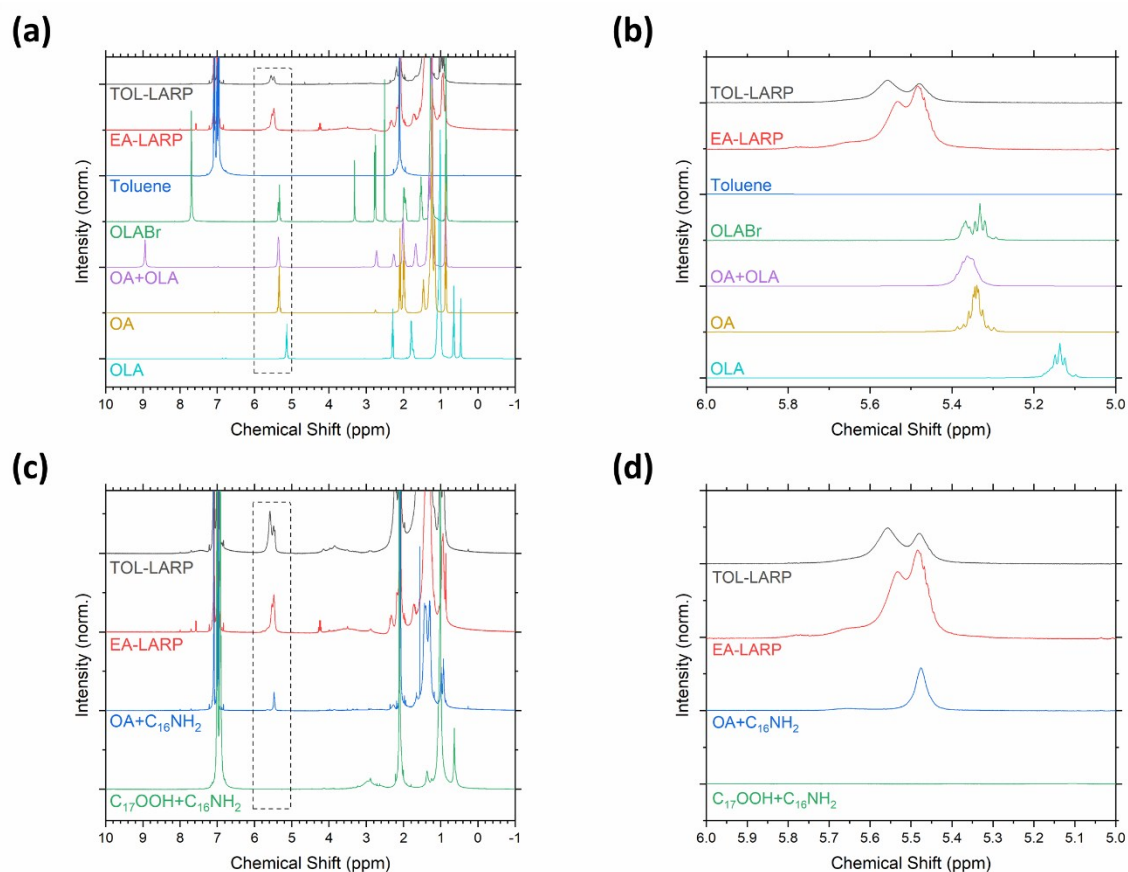


Figure S16. (a) $^1\text{H-NMR}$ spectra of purified PNCs from TOL/EA-LARP and the reference spectra of possible species that could interact with the CsPbBr_3 surface, as well as neat-toluene to track residues of non-deuterated toluene. (b) Size enhancement of the dotted region in (a) containing the pair of broad chemical shifts of 5.4-5.6 ppm which are indicative of the alkene $\text{C}=\text{C}$ protons of surface binding oleyl species. While the reference spectra for the individual OA and OLA ligands display peak splitting, their combined $\text{OLA}^+\text{-OA}^-$ salt product results in a single broad peak centered at 5.36 ppm. When the OLA^+ and OA^- ligands were present with the CsPbBr_3 PNCs, both peaks became visible. These twin peaks are slightly shifted downfield compared to the references, indicating the interactions with the PNC surface are shielding their protons. (c, d) To ensure that these signals indeed correspond to the $\text{C}=\text{C}$ protons interacting with

the PNC surface, an alkene free synthesis of CsPbBr₃ was performed with heptadecanoic acid (C₁₇OOH) and hexadecylamine (C₁₆NH₂). An accompanying synthesis using OA and C₁₆NH₂ confirmed that the C=C peak at 5.48 ppm is from OA⁻, and that the other peak at 5.53-5.55 ppm is from OLA⁺. This confirms that for both LARP methods, the PNCs are passivated by OLA⁺ with predominantly an accompanying OA⁻ species. Nonetheless, it still remains possible and likely that Br⁻ is also a counter-ion,² given the PbBr₂ terminated surface.

11. FTIR Spectroscopy

Fourier transform infra-red (FTIR) spectroscopy was performed with a Smart iTR™ Attenuated Total Reflectance (ATR) Sampling Accessory attachment. The organic ligands were analyzed in their liquid state, while the oleylammonium bromide salt was analyzed in its solid form. The CsPbBr₃ nanocrystals were analyzed in its solid state by depositing concentrated PNC solutions directly onto the plate and allowing the toluene solvent to evaporate, leaving the PNCs behind.

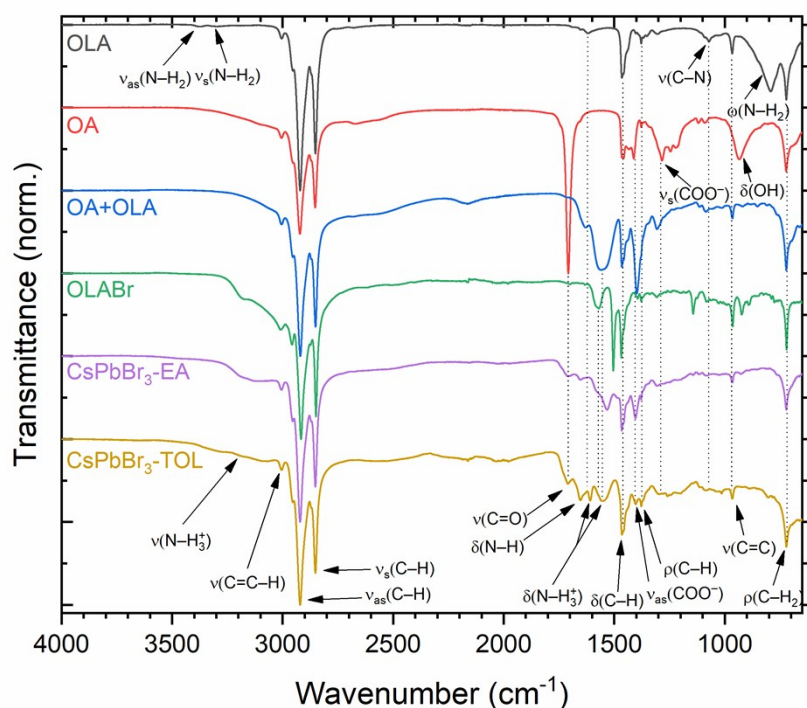


Figure S17. To probe the surface chemistry of the PNCs, fourier-transform infrared (FTIR) spectroscopy compared the purified CsPbBr₃ PNCs against the individual starting ligands of OA, OLA, and their possible binding products of oleylammonium-oleate (OA⁺-OLA⁻) and oleylammonium bromide (OLABr). Both TOL- and EA-LARP synthesized PNCs share comparable FTIR spectra. Centered at ~3165 cm⁻¹ is a weak band attributed to the ν(N-H) vibrational mode from OLABr. Additional bending δ(N-H) modes of an OLA⁺ salt with OA⁻ or Br⁻ are visible between 1534-1609 cm⁻¹ as generally broad peaks. A slightly upshifted δ(N-H) scissoring peak at 1652 cm⁻¹ compared to that of OLA at 1623 cm⁻¹ is also observed. The strong ν(C=O) peak of OA at 1706 cm⁻¹ is weakened and broadened upon conversion to OA⁻ and is observed in the PNCs at 1710-1712 cm⁻¹. The remaining peaks relate to the stretching, bending or rocking modes of carbon-carbon or carbon-hydrogen moieties of alkenes or alkanes at 2852-3006, 1465, 1377, 967 and 721 cm⁻¹. These results suggest that the active binding species are OA⁺-OLA⁻, OLABr or both.

12. Post-synthetic Treatments to CsPbBr₃ PNCs

For Figure 4a,b; the synthesized alkylammonium bromide salts were added to anhydrous-IPA at 1.0 mg/mL and sonicated until fully dissolved. These IPA-ligand solutions were sequentially added to a cuvette containing 35 μ g (60 nmol) of CsPbBr₃ PNCs, from the same purified TOL-LARP solution dispersed in 3.0 mL of toluene. After each addition, the cuvette was gently hand agitated for 30 s and left to stand for another 30s before each measurement. In all other cases (e.g. Figure 4c,d), treatments used a toluene-based ligand solution where the salts were prepared at 1.0 mg/mL. Temporarily heating the solutions to \sim 60 $^{\circ}$ C was necessary to solubilize the salts, and then allowed to return to room temperature before use. The only exception was C₁₆NH₃Br, where it's solubility limit rendered its concentration instead to be at 0.5 mg/mL.

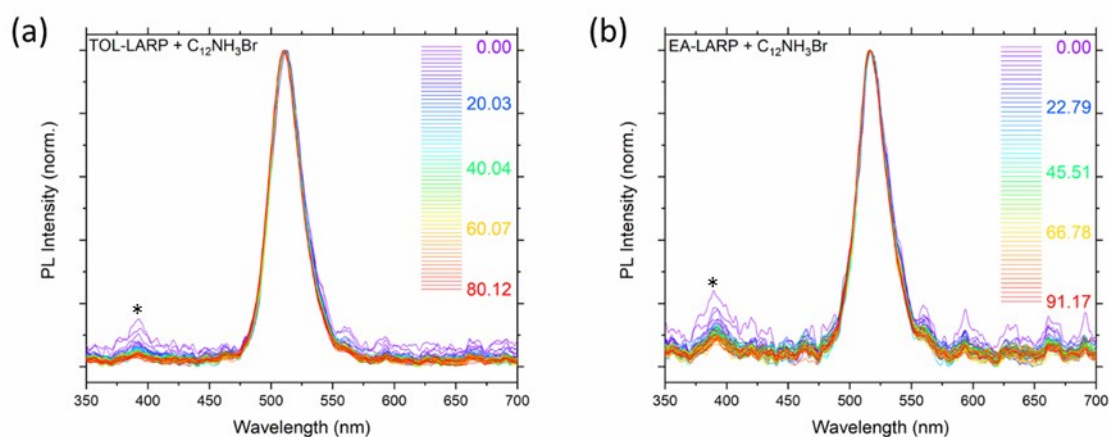


Figure S18. The normalized TD-PL spectra of the two-step addition, of 20 μ g then 100 μ g, of C₁₂NH₃Br (total 120 μ g) to purified (a) TOL-LARP and (b) EA-LARP synthesized CsPbBr₃ PNCs solutions. ‘*’ indicates 390 nm scattering from the LED source.

13. EA-LARP Syntheses with Primary Saturated Alkylamines

For the different EA-LARP variants using saturated primary amines, OLA is replaced with an equimolar quantity to retain the acid:amine molar ratio at 2:1. No other changes to the standard EA-LARP reaction conditions and purification protocol were made (Figure S19). The exception is for the variant using butylamine, where its DMF precursor was not heated and kept at room temperature, as the ligand was fully soluble and the precursor homogeneous. Performing the synthesis with the precursor heated to 80 $^{\circ}$ C resulted in more colloiddally unstable crystals. This was attributed to a reduction in amine content due to its low boiling point during heating, or from the enhanced growth kinetics. As a result of the inverse relationship between the chain length and solubility in EA, it was found that C₁₆NH₂ with OA forms a white precipitate of their salt despite the low concentration required for synthesis (Figure S20). The initial crude solutions are similar in their absorbance profiles, but due to the non-optimized purification protocols and differing ligand solubilities, the purified samples are noticeably different in their absorption band edges. The fraction of perovskite material distributed in the purified solutions and the discarded waste from the purification steps can be estimated from their optical densities (Figure S21, Table S4). The main optical features of interest for their purified solutions and yields are tabulated in Table S5.

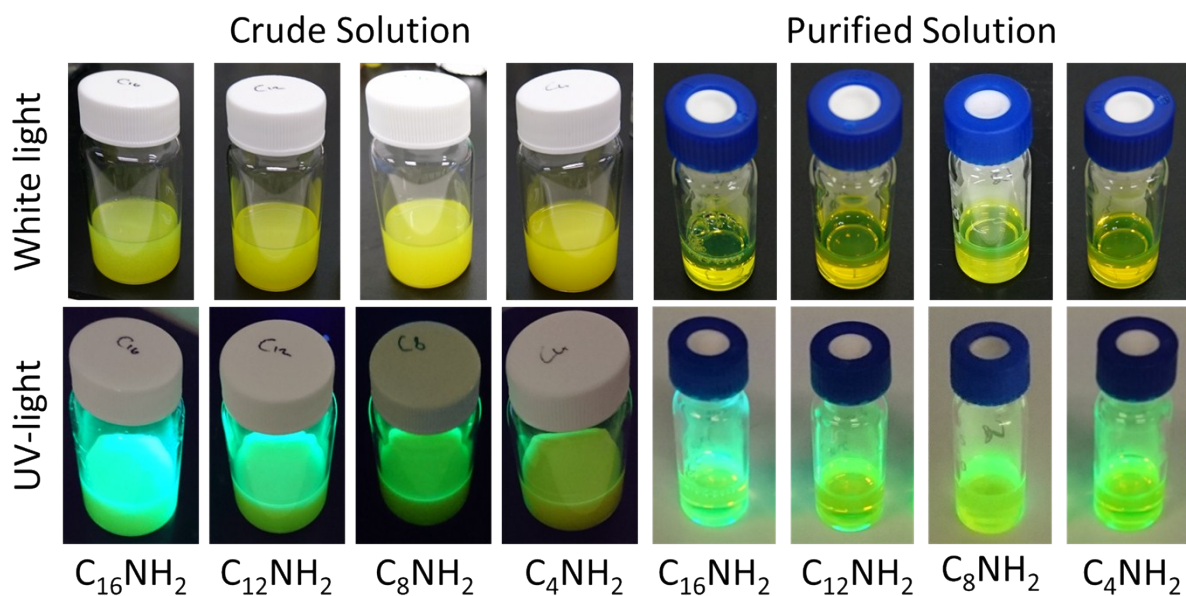


Figure S19. Photographs of the crude and purified solutions of EA-LARP solutions made with saturated primary amines in lieu of OLA under white light and $\lambda = 365$ nm UV light.

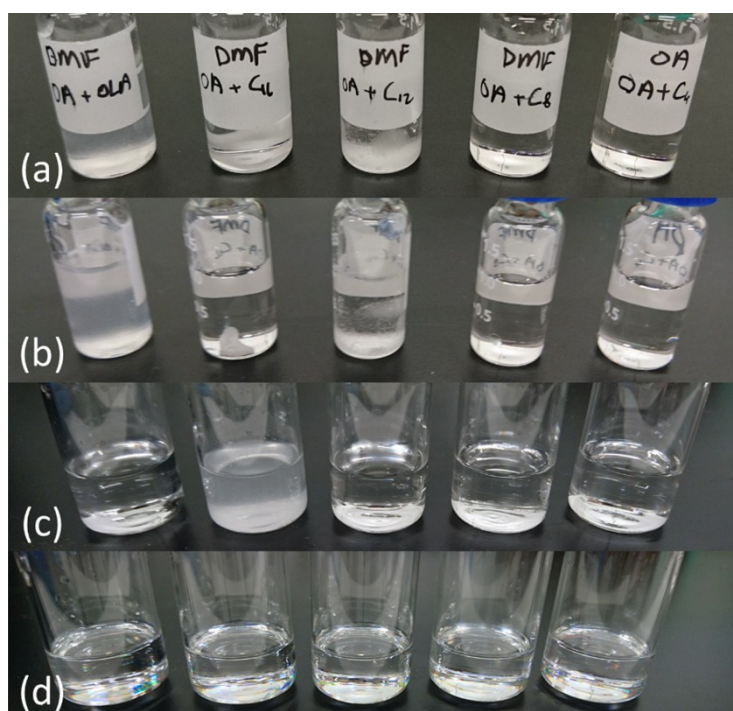


Figure S20. (a,b) Neat-DMF with the different acid:amine combinations (room temperature) at the concentrations used for EA-LARP synthesis added into (c) EA and (d) TOL. All solutions are clear except for EA with $C_{16}NH_2$, indicating that most combinations are not limited by ligand solubility issues.

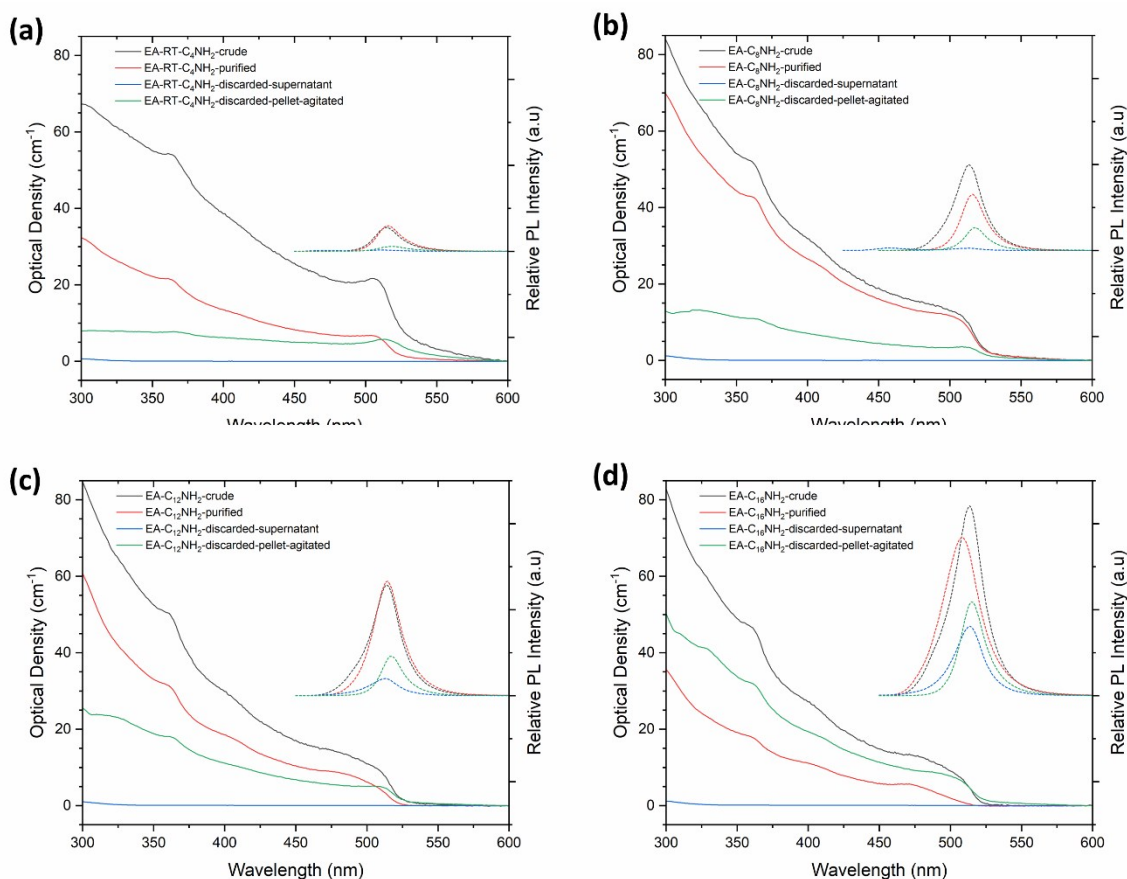


Figure S21. The optical density (solid curve) derived from absorbance measurements and PL (dotted curve) spectra of EA-LARP synthesized CsPbBr₃ PNCs with the saturated amine ligand (a) C₁₆NH₂, (b) C₁₂NH₂, (c) C₈NH₂ and (d) C₄NH₂ substituting for OLA, with all other conditions left identical unless specified. The absorbance and PL spectra of the (e) crude and (f) purified solutions of the different amine synthesized variants, with C₈NH₂ showing the highest yield.

Table S4: Estimations of perovskite content from their optical density relative to their measured crudes.

Optical Density	Purified Solution	Discarded Supernatant	Discarded Pellet	Σ
Tol-OLA	23.9 %	12.4 %	45.2 %	81.5 %
EA-OLA	60.2 %	21.6 %	19.5 %	101.3 %
EA-C ₁₆ NH ₂	39.4 %	0.4 %	72.8 %	112.6 %
EA-C ₁₂ NH ₂	62.1 %	0.3 %	37.8 %	100.2 %
EA-C ₈ NH ₂	83.1 %	0.2 %	22.1 %	105.4 %
EA-C ₄ NH ₂	45.7 %	0.1 %	14.5 %	60.3 %

Table S5: Summarization of absorption and PL properties of purified EA-LARP solutions using saturated amines and their reaction yield and their yield using ICP-MS data and the molar extinction coefficient.

Purified Solutions	C ₁₆ NH ₂	C ₁₂ NH ₂	C ₈ NH ₂	C ₄ NH ₂
PL Peak (nm)	508	514	516	516
PL fwhm (nm)	30	23	20	21
Abs onset (nm)	~525	~528	~529	~529
Abs 1 st excitonic peak (nm)	~471	~495	~505	~506
CsPbBr ₃ Reaction Yield (%)	33.3	56.1	70.1	37.5
PNC mass per waste volume (mg/mL)	0.52	0.87	1.08	0.58

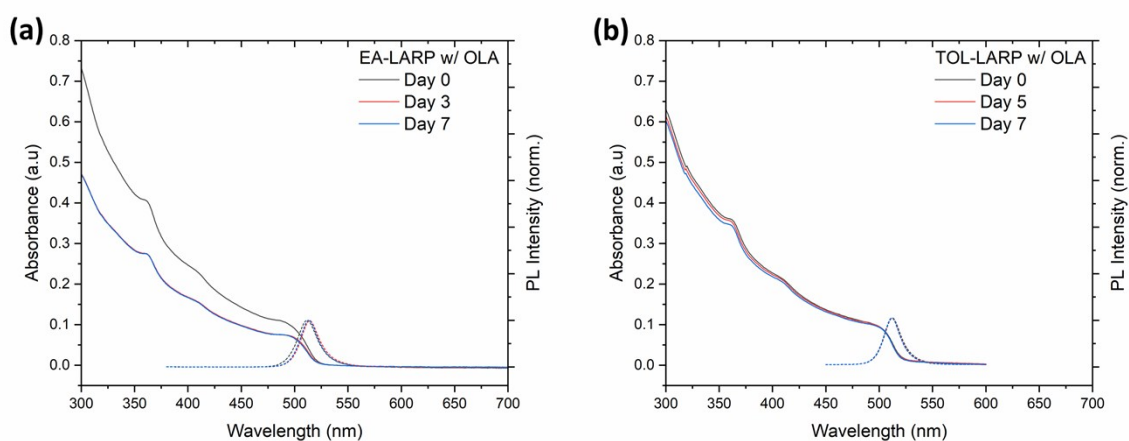


Figure S22. (a) The absorption (solid curve) and PL (dotted curve) spectra showing the colloidal stability of (a) EA-LARP and (b) TOL-LARP over a week without any post-ligand additives. Note, the TOL-LARP sample has a dilution factor of 150, rather than EA-LARP's dilution factor of 300, to roughly equalize the concentration of PNCs due to EA-LARP's higher yield.

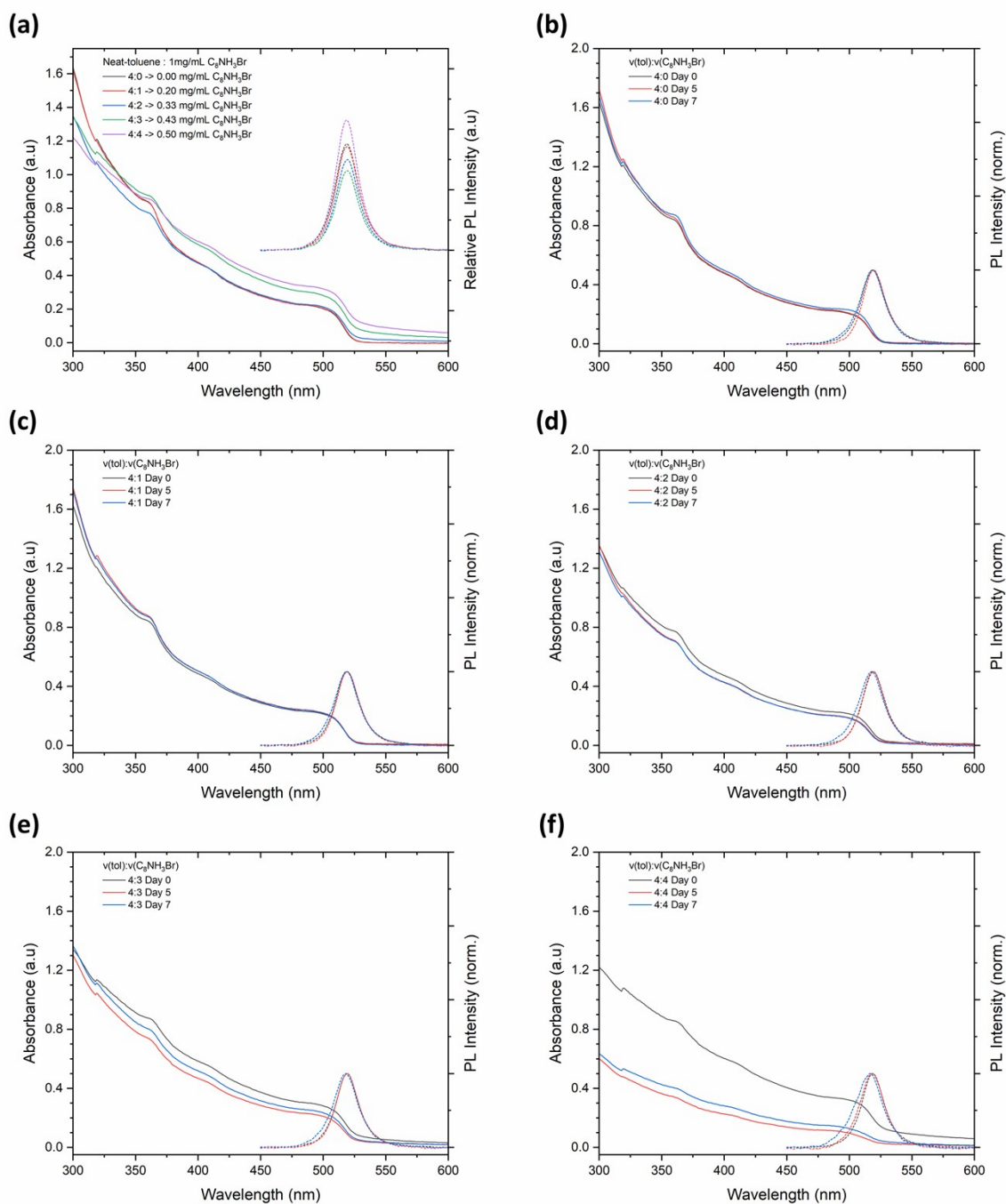


Figure S23. (a) The absorption (solid curve) and PL (dotted curve) spectra showing the influence of increasing concentration of C_8NH_3Br additives into purified EA-LARP solution which used C_8NH_2 as the starting amine instead of OLA. Similarly, the spectra of individual samples from Figure S23a taken over a week, with the respective C_8NH_3Br concentrations are (b) 0 mg/mL, (c) 0.20 mg/mL, (d) 0.33 mg/mL, (e) 0.43 mg/mL and (f) 0.50 mg/mL.

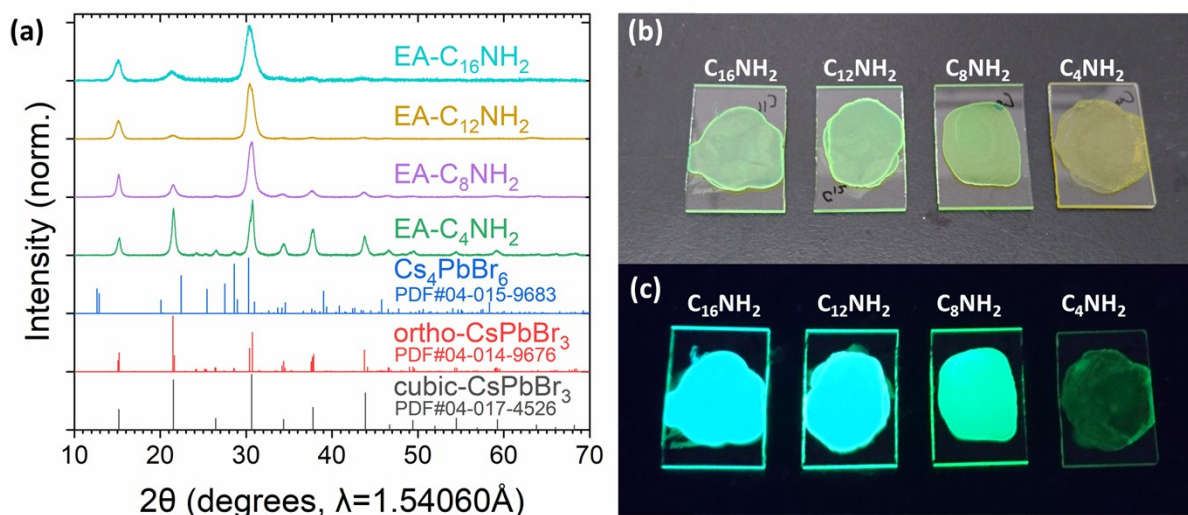


Figure S24. (a) XRD patterns of the purified EA-LARP solutions using different saturated alkylamines in lieu of OLA for synthesis. The respective XRD film samples under (b) ambient light (top) and (c) $\lambda = 365$ nm UV-light (bottom).

14. Upscaling EA-LARP

For upscaling, 30 mL of DMF precursor using C₈NH₂ was added to 450 mL of EA and used identical purification steps as with usual small scale samples.



Figure S25. Small scale (left) and upscaled crude solutions under (a) ambient light and (b) $\lambda = 365$ nm UV-light. Pellets and waste solvent after first centrifugation of (c) small scale and (d) upscaled reactions. (e) Purified CsPbBr₃ nanocrystal solution of upscaled reaction. Purified nanocrystal solutions of small scale (left) and upscaled (right) reactions under (f) ambient light and (g) $\lambda = 365$ nm UV-light.

15. Halide Exchange

Chloride (PbCl_2 co-solubilized with OA and OLA in toluene) and iodide (PbI_2 co-solubilized with OA and OLA in toluene) exchange solutions were added to EA-LARP synthesized PNCs for halide exchange in toluene solvent. Static absorbance and PL measurements were made using the Perkin Elmer Lambda 950 UV-Vis-NIR spectrometer and Horiba Fluoromax-4 Spectrofluorometer, respectively. Time-dependent PL measurements were made using the StellarNet spectrometer, where a $\sim 10:1$ molar ratio of excess Cl^- or I^- was rapidly injected into a 2000 rpm stirred cuvette of CsPbBr_3 PNCs.

16. References

- 1 Y. Bekenstein, B. A. Koscher, S. W. Eaton, P. Yang and A. P. Alivisatos, *J. Am. Chem. Soc.*, 2015, **137**, 16008–16011.
- 2 F. Krieg, S. T. Ochsenbein, S. Yakunin, S. ten Brinck, P. Aellen, A. Süess, B. Clerc, D. Guggisberg, O. Nazarenko, Y. Shynkarenko, S. Kumar, C.-J. Shih, I. Infante and M. V. Kovalenko, *ACS Energy Lett.*, 2018, **3**, 641–646.
- 3 R. F. Kubin and A. N. Fletcher, *J. Lumin.*, 1982, **27**, 455–462.
- 4 L. Protesescu, S. Yakunin, M. I. Bodnarchuk, F. Krieg, R. Caputo, C. H. Hendon, R. X. Yang, A. Walsh and M. V. Kovalenko, *Nano Lett.*, 2015, **15**, 3692–3696.
- 5 J. De Roo, M. Ibáñez, P. Geiregat, G. Nedelcu, W. Walravens, J. Maes, J. C. Martins, I. Van Driessche, M. V. Kovalenko and Z. Hens, *ACS Nano*, 2016, **10**, 2071–2081.
- 6 J. Maes, L. Balcaen, E. Drijvers, Q. Zhao, J. De Roo, A. Vantomme, F. Vanhaecke, P. Geiregat and Z. Hens, *J. Phys. Chem. Lett.*, 2018, **9**, 3093–3097.